(LATE)

Essential Ingredients for Modeling of Hot-Carrier Degradation in Ultra-Scaled MOSFETs

Stanislav Tyaginov*, Markus Bina*, Jacopo Franco°, Dmitri Osintsev*, Yannick Wimmer*,
Ben Kaczer°, and Tibor Grasser*
*Institute for Microelectronics, Vienna University of Technology, Gußhausstraße 27-29, A-1040 Wien, Austria
° imec, Kapeldreef 75, 3001 Leuven, Belgium
Email: tyaginov@iue.tuwien.ac.at

***Abstract*—We present a novel approach to hot-carrier degradation (HCD) simulation, which for the first time considers and incorporates mechanisms crucial for HCD. First, two main pathways of Si-H bond dissociation, namely bond-breakage triggered by a single hot carrier and induced by multivibrational bond excitation, are combined and considered consistently. Second, we show how drastically electron-electron scattering affects the whole HCD picture. Furthermore, dispersion of the activation energy of bond dissociation substantially changes defect generation rates. Finally, the interaction between the electric field and the dipole moment of the bond leads to interface states created near the source end of the channel. To demonstrate the importance of all these peculiarities we use ultra-scaled n-MOSFETs with a channel gate of 65 nm.**

I. Introduction

Hot-carrier degradation (HCD) is known to be severe even in ultra-scaled devices where carriers are unlikely to gain energy sufficient for generation of interface states via dissociation of Si-H bonds in a single collision [1, 2]. Two main reasons for this are the multivibrational excitation (MVE) of the bond [3–5] and scattering mechanisms populating the high energetical fraction of the carrier ensemble [6, 7]. Among the scattering mechanisms, electron-electron scattering (EES) plays the most crucial role beyond the 180 nm node [8, 9]. This tendency demonstrates that while device dimensions shrink the situation substantially changes on both the microscopic and the carrier transport level.

As we have demonstrated in our previous publications [10–12], microscopic mechanisms and carrier transport are essential aspects of the HCD phenomenon. Therefore, for a proper modeling and understanding of HCD in ultra-scaled devices one has to essentially consider MVE and EES mechanisms at the corresponding levels. From a simulation perspective, the MVE process has to be combined with another mechanism of bond dissociation, when bond rupture is directly triggered by a solitary energetical carrier via excitation of one of the bonding electrons to an antibonding state (this process is further marked as AB) [13]. As for carrier transport, EES changes the carrier energy distribution function, and thus is crucial for HCD modeling in nanoscale MOSFETs [8, 14].

Although, the importance of both MVE and EES mechanisms has been discussed in literature [3, 9, 13–16], their proper implementation into an HCD model has been lacking. In most approaches the so-called "energy-driven paradigm" proposed by Rauch and LaRosa has been used [14]. This concept is based on a simplified treatment of carrier transport where information on the carrier distribution is represented by condition related empirical factors. For instance, in the model developed by the group of Bravaix, three main modes governed by the AB mechanism, EES, and MVE process are distinguished [15, 16]. Such a description of HCD may be a severe approximation these mechanisms affect each other and have to be considered consistently [10, 11].

In our previous attempts, which were based on thorough carrier transport treatment using a solution of the Boltzmann transport equation [10–12], the AB and MVE processes are considered as independent. The resulting concentration of interface states (N_{it}) was calculated as a superposition of AB and MVE related densities weighted with probability factors. Such an approach, however, is not physically reasonable because AB and MVE mechanisms are different pathways of the same reaction, of Si-H bond dissociation. Independently of a particular pathway, the reaction converts the same precursors (virgin bonds) into same interface traps (P_{b} centers). Therefore, the AB and MVE mechanisms have to be considered as competing within the same rate equation. Moreover, their rates are defined by the carrier energy distribution function which has to be calculated for each particular device geometry and stress conditions.

Another important factor which affects the dissociation rate is the dispersion of the bond-breakage activation energy as observed in ESR experiments [17]. Statistical variations of this quantity were shown to be crucial for modeling of the intimately related phenomenon, of bias temperature instability [18, 19]. As for HCD, the impact of the activation energy distribution on the time slope of transistor characteristics degradation was discussed in [20]. However, to our best knowledge, this information was not integrated into any physics-based model of HCD.

The activation energy for the bond dissociation can also be effectively changed due to the interaction between the dipole moment of the bond and the electric field [21, 22]. Under real stress/operating conditions the electric field is non-homogeneously distributed in the transistor channel. As a result, the corresponding reduction in the activation energy is also a laterally distributed quantity. At the same time, HCD is a severely non-uniform phenomenon with the maximum N_{it} near the drain end of the gate [6, 7], since carriers need to gain energy sufficient for triggering a bond rapture event. With the

978-1-4799-0352-8/13/$31.00 ©2013 IEEE

reduction of the activation energy due to the electric field the trade-off between this reduction and formation of a prominent high energetical fraction of the carrier ensemble can lead to another $N_{\rm it}$ peak shifted towards the source with respect to the "traditional" one. Since the device performance is more sensitive to interface states created closer to the transistor center, the aforementioned reduction of activation energy can play a substantial role in HCD.

To conclude, such peculiarities as the consistent consideration of AB and MVE mechanisms, the effect of EES on the carrier energy distribution function, the activation energy dispersion, and its reduction due to the interaction of the bond dipole moment with the electric field are essential ingredients of the physics-based HCD model. In this abstract we incorporate all these peculiarities into our approach, verify the model and demonstrate the importance of these peculiarities.

II. Experiment

lufthansa We employ n-MOSFETs with a gate length of 65 nm. A 2.5 nm SiON film was grown by decoupled plasma nitridation followed by post-nitridation anneal. These short-channel transistors were subjected to hot-carries stress in the worst-case regime, i.e. at $V_{\rm gs} = V_{\rm ds}$ [5, 23]. To prominently demonstrate the impact of the main model ingredients on HCD we have chosen particular conditions with $V_{\rm gs} = V_{\rm ds} = 1.8$ V at an ambient temperature of 298 K. The devices were stressed for ∼8.8 ks. Interface states generated during stress perturb the electrostatics of the device and degrade the carrier mobility. To assess HCD we used the relative change of the linear drain current $\Delta I_{\rm dlin}$ (measured at $V_{\rm gs}$=1.5 V and $V_{\rm ds}$=0.05 V), see Fig. 1.

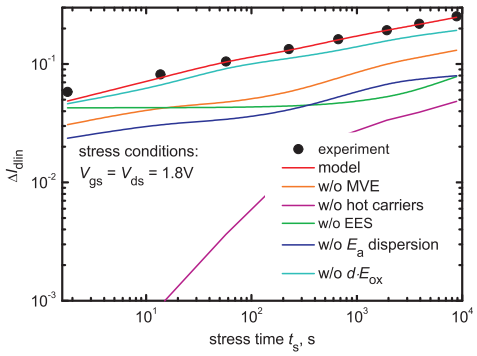

Fig. 1. The linear drain current $\Delta I_{\rm dlin}$ change as a function of stress time: experiment (the device is stressed at $V_{\rm gs} = V_{\rm ds} = 1.8$ V and T = 300 K) vs. simulations. With all ingredients included the model represents the experimental $\Delta I_{\rm dlin}(t)$ curve. For comparison, $\Delta I_{\rm dlin}(t)$ simulated disregarding EES, AB, MVE mechanisms, activation energy dispersion, and its reduction due to the interaction of the dipole moment with electric field are plotted.

III. The Model

Our physics-based HCD model consists of three different subtasks: microscopic description of defect build-up, carrier transport treatment, and modeling of the degraded devices [10, 12]. For the two last subtasks the deterministic solver of the Boltzmann transport equation ViennaSHE [12, 24] is used.

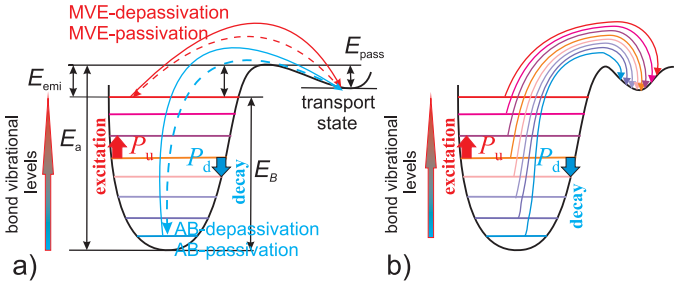

Fig. 2. The Si-H bond as a truncated harmonic oscillator. In (a) only bond dissociation from the ground state (via excitation of one of the bonded electrons to an antibonding state) and from the last bonded state (via the pure multivibrational excitation) are considered. (b) demonstrates that first the bond can be heated by the MVE process to the $i^{\rm th}$ level followed by the H release from this level induced by the AB process.

ViennaSHE calculates the carrier energy distribution functions for a particular device architecture and stress/operating conditions, considering scattering at ionized impurities, impact ionization, electron-phonon, and electron-electron scattering as well as full-band effects. This information is then used to calculate the carrier acceleration integral, which defines the cumulative ability of the carrier packet to dissociate bonds [10]. As for the microscopic picture of HCD, the Si-H bond is considered as a truncated harmonic oscillator, see Fig. 2. However, in contrast to our previous approach [10, 12], we follow the scenario proposed within the Hess model [3] and consider a superposition of MVE and AB mechanisms. In the last version of our model only two limiting cases of bond rupture from the ground state and from the last bonded level were regarded, Fig. 2,a. These mechanisms correspond to bond rupture by a single energetical carrier and by a series of colder carriers. Within the current model, we consider all combinations of MVE and AB processes. In other words, first the bond can be heated by several colder carriers to an excited level followed by the hydrogen release triggered by a solitary hot particle Fig. 2,b.

Mathematically, this means that the system of rate equations for the oscillator has to be modified in a manner to include the bond passivation/depassivation rates to/from all the states:

$$\begin{aligned}
\frac{{\rm d}n_0}{{\rm d}t} &= P_{\rm d} n_1 - P_{\rm u} n_0 - R_{{\rm a},0} n_0 + R_{{\rm p},0} N_{\rm it}^2 \\
\frac{{\rm d}n_i}{{\rm d}t} &= P_{\rm d}(n_{i+1} - n_i) - \\
&\quad -P_{\rm u}(n_i - n_{i-1}) - R_{{\rm a},i} n_i + R_{{\rm p},i} N_{\rm it}^2 \\
\frac{{\rm d}n_{N_l}}{{\rm d}t} &= P_{\rm u} n_{N_l - 1} - P_{\rm d} n_{N_l} - R_{{\rm a},N_l} n_{N_l} + R_{{\rm p},N_l} N_{\rm it}^2,
\end{aligned} \tag{1}$$

where n_i is the level occupation number, N_l the index of the last bonded level, $P_{\rm u}$,$P_{\rm d}$ the bond excitation/deexcitation rates, while $R_{{\rm a},i}$ and $R_{{\rm p},i}$ denote the bond rupture/passivation rates from the $i^{\rm th}$ level, respectively (see [25] for more detail). The bond heating/cooling rates $P_{\rm u}/P_{\rm d}$ are defined by the carrier acceleration integral ($I_{\rm MVE}$) for the MVE process [10, 25].

Similarly to [5, 25], we solve (1) by assuming a large disparity between the characteristic times for establishing of the oscillator steady-state and bond passivation/depassivation

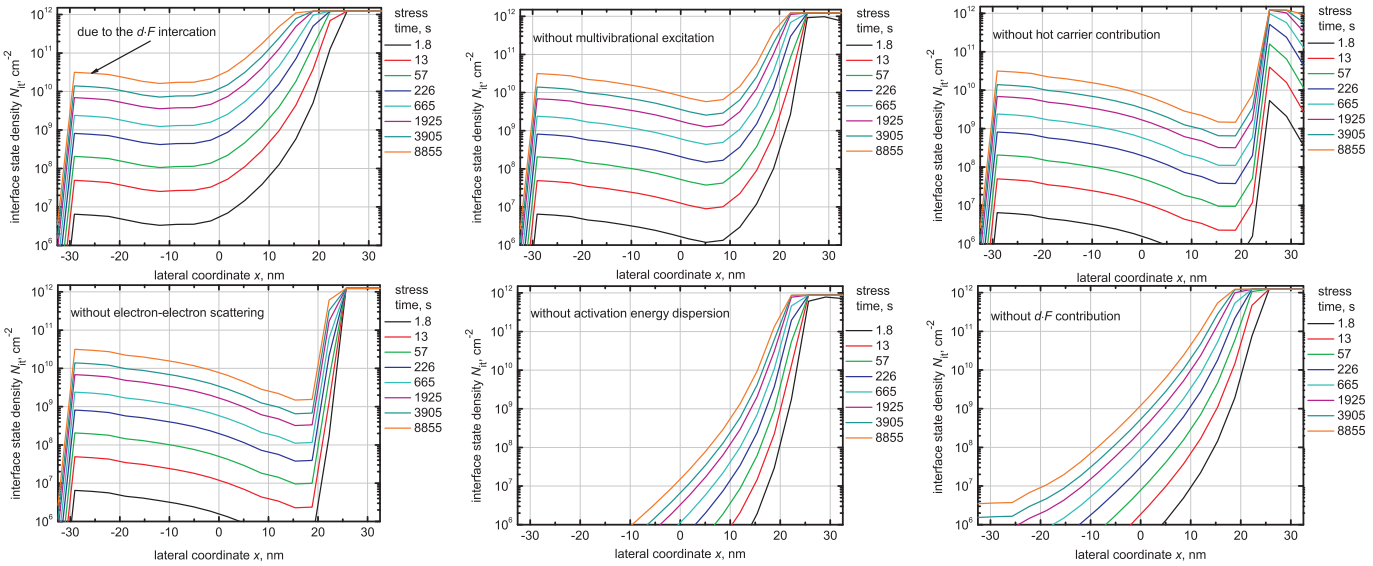

Fig. 3. Interface state density profiles $N_{\rm it}(x)$ calculated using the calibrated model regarding/disregarding all the essential mechanisms: MVE, AB, EES, the dispersion of the activation energy for bond dissociation, and the reduction of this energy due to the interaction between the bond dipole moment and the electric field.

processes.

$$\frac{{\rm d}N_{\rm it}}{{\rm d}t} = (N_0 - N_{\rm it})\,\Re_{\rm a} - N_{\rm it}^2 \Re_{\rm p}, \tag{2}$$

where N_0 is the density of Si-H bonds and $\Re_{\rm a}$, $\Re_{\rm p}$ are:

$$\Re_{\rm a} = \frac{1}{k}\sum_i R_{{\rm a},i}\left(\frac{P_{\rm u}}{P_{\rm d}}\right)^i, \quad \Re_{\rm p} = \sum_i R_{{\rm p},i} \tag{3}$$

with k being the normalization factor, $k^{-1} = \sum (P_{\rm u}/P_{\rm d})^{\rm i}$. The solution of (2) reads:

$$N_{\rm it}(t) = \frac{\sqrt{\Re_{\rm a}^2 + N_0\Re_{\rm a}\Re_{\rm p}}}{\Re_{\rm p}}\frac{1-f(t)}{1+f(t)} - \frac{\Re_{\rm a}}{\Re_{\rm p}},$$
$$f(t) = \frac{\sqrt{\Re_{\rm a}^2 + N_0\Re_{\rm a}\Re_{\rm p}} - \Re_{\rm a}}{\sqrt{\Re_{\rm a}^2 + N_0\Re_{\rm a}\Re_{\rm p}} + \Re_{\rm a}} \times \tag{4}$$
$$\times \exp\left(-2t_{\rm s}\sqrt{\Re_{\rm a}^2 + N_0\Re_{\rm a}\Re_{\rm p}}\right)$$

The dissociation rate $R_{\rm a,i}$ from the $i^{\rm th}$ level with energy $E_{\rm i}$ are defined as

$$R_{{\rm a},n_i} = I_{{\rm AB},i} + w_{\rm th}\exp\left[-\left(E_{\rm a} - E_i\right)/k_{\rm B}T\right], \tag{5}$$

here the latter term represents the thermal activation over the potential barrier $E_{\rm a} - E_i$ (Fig. 2) separating the bonded state and the transport mode, while the acceleration integral

$$I_{{\rm AB},i} = \int_{E_{\rm th}}^{\infty} f(E)g(E)\sigma_0(E - E_{\rm a} + E_i)^p v(E){\rm d}E, \tag{6}$$

represents the bond-breakage rate induced by hot carriers (for more detail, see [25]).

We assume that the activation energy for bond dissociation is a normally distributed quantity [17, 26]. The mean value and the standard deviation used in the model are 1.5 eV and 0.15 eV, respectively, and close to those reported in [17, 26].

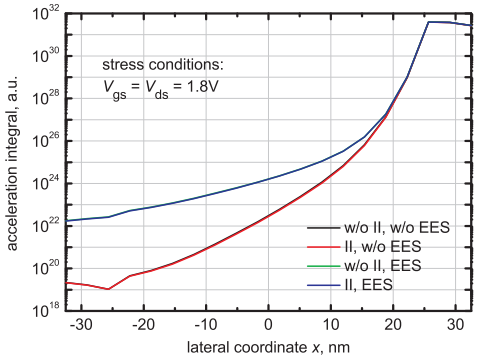

Fig. 4. The carrier acceleration integral calculated for the ground state regarding/disregarding impact ionization and electron-electron scattering. One concludes that the former one does not change the acceleration integral significantly, while the latter one substantially impacts the acceleration integral.

The activation energy $E_{\rm a}$ can also change due to the interaction of the Si-H bond dipole moment with the electric field [21, 22]. This energy reduction is calculated as $d \cdot E_{\rm ox}$ using the approach presented in [22].

IV. Results and Discussion

The model was calibrated in a manner to represent the time dependence $\Delta I_{\rm dlin}(t)$. Fig. 1 demonstrates that agreement between experimental and simulated (considering all the aforementioned ingredients: EES, MVE, AB, dispersion of the activation energy, and its reduction due to the $d \cdot E_{\rm ox}$ interaction) $\Delta I_{\rm dlin}(t)$ curves is good. If we ignore one of these ingredients, the simulated $\Delta I_{\rm dlin}(t)$ dependence dramatically deviates from the experimental one.

Corresponding $N_{\rm it}(x)$ profiles are plotted in Fig. 3, while the acceleration integral calculated for the stress conditions and for the ground state, i.e. for $E_i = 0$ in (6), regarding/disregarding impact ionization and electron-electron scattering is plotted in Fig. 4. One can see that impact ionization

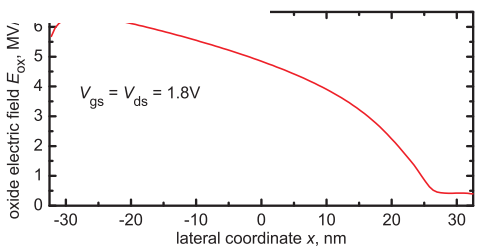

Fig. 5. The oxide electric field calculated at the Si/SiON interface for the stress conditions as a function of the lateral coordinate x.

does not significantly change the acceleration integral, while the impact of EES is substantial and the effect becomes more pronounced closer to the source. This tendency is visible also in Fig. 3 where $N_{\rm it}(x)$ profiles calculated disregarding EES demonstrate a prominent valley between source and drain maxima. The "main" drain maxima becomes wider as we take EES into account, thereby reflecting the tendency visible in Fig. 4.

As for the source $N_{\rm it}$ peak, it is related to the $d \cdot E_{\rm ox}$ activation energy reduction. Fig. 5 demonstrates the electric field profile at the Si/SiON interface calculated for the stress conditions. One can see that the electric field is high and its maximum is located in the vicinity of the source junction, thereby making the activation energy reduction most pronounced in this area. As for the effect of $E_{\rm a}$ statistical variations, its dispersion considerably affects the $N_{\rm it}(x)$ profile except close to drain where carriers are hot enough, see Fig. 3. Note that local variations of the activation energy also varies the depth of the quantum well, and hence the number of eigenstates. This tendency is reflected by the acceleration integral profiles plotted for all states according to (6), see Fig. 6. Since the electric field is relatively weak near the drain end of the gate, the impact of $d \cdot E_{\rm ox}$ is less pronounced there. As a result, the quantum well is deepest in this device area and highest bonded levels (with corresponding acceleration integral profiles) appear only at $x > 15$ nm, see Fig. 6.

Comparison of $\Delta I_{\rm dlin}(t)$ curves evaluated ignoring either MVE or AB contributions (Fig. 1) suggest that the AB process has a much stronger impact on the drain current. This is confirmed by the $N_{\rm it}$ profiles. Such a result is not surprising because stress voltages are high enough in order to accelerate carriers up to substantially high energies.

V. Conclusion

Our physics-based HCD model has been refined in a manner to consistently consider and combine hot and cold carrier contributions to bond dissociation. The system of the rate equations has been modified accordingly and the analytical expression for the concentration $N_{\rm it}$ has been derived. We have demonstrated that at relatively high stress voltages of 1.8 V even in the case of the worst-case scenario for the ultra-scaled MOSFET, the damage is still governed by the hot-carrier mechanism. This mechanism is additionally reinforced by EES. Also, the $E_{\rm a}$ dispersion considerably strengthens HCD. Variation of this energy is also induced by the interaction

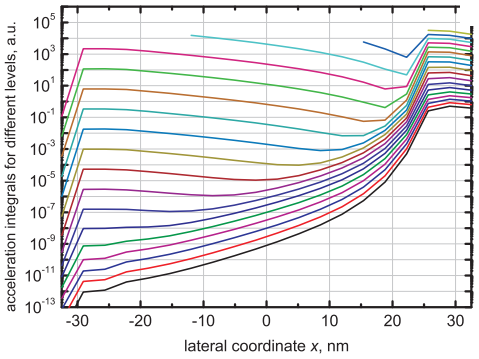

Fig. 6. The carrier acceleration integrals for each level of the oscillator calculated disregarding the activation energy dispersion for a fixed energy $E_{\rm a}$ equal to the mean value but considering the $d \cdot E_{\rm ox}$ energy reduction. The electric field becomes stronger closer to the source, making the quantum well shallower. As a result, some acceleration integral profiles are visible only near the drain end of the gate where $E_{\rm ox}$ is relatively weak.

between the bond dipole moment and the electric field. This effect leads to a secondary peak of $N_{\rm it}(x)$ pronounced near the source.

Acknowledgment

The authors acknowledge support by the Austrian Science Fund (FWF), grant P23598.

References

[1] F.-C. Hsu *et al.*, IEEE Electron Dev. Lett. **5**, 148 (1984).
[2] T. Mizuno *et al.*, *Proc. International Electron Devices Meeting (IEDM)* (1992), pp. 695–698.
[3] W. McMahon *et al.*, *Proc. Int. Conf. Mod. Sim. Micro* (2002), Vol. 1, pp. 576–579.
[4] W. McMahon *et al.*, IEEE Trans. Nanotech. **2**, 33 (2003).
[5] A. Bravaix *et al.*, *Proc. International Reliability Physics Symposium (IRPS)* (2009), pp. 531–546.
[6] A. Bravaix *et al.*, *Proc. European Symposium on Reliability of Electron Devices Failure Physics and Analysis (ESREF), tutorial* (2010).
[7] S. Rauch *et al.*, *Proc. International Reliability Physics Symposium (IRPS), tutorial* (2010).
[8] P. Childs *et al.*, IEEE Electron Dev. Lett. **31**, 139 (1995).
[9] S. Rauch *et al.*, IEEE Electron Dev. Lett. **19**, 463 (1998).
[10] S. Tyaginov *et al.*, *Proc. International Conference on Simulation of Semiconductor Processes and Devices (SISPAD)* (2011), pp. 123–126.
[11] S. Tyaginov *et al.*, *Proc. International Integrated Reliability Workshop (IIRW)* (2012), pp. 206–215.
[12] M. Bina *et al.*, *Proc. International Electron Devices Meeting (IEDM)* (2012), pp. 713–716.
[13] K. Hess *et al.*, Physica E **3**, 1 (1998).
[14] S. Rauch *et al.*, *Proc. International Reliability Physics Symposium (IRPS)* (2005).
[15] C. Guerin *et al.*, IEEE Trans. Dev. Material. Reliab. **7**, 225 (2007).
[16] Y. Randriamihaja *et al.*, Microel. Reliab. **52**, 2513 (2012).
[17] A. Stesmans, Appl. Phys. Lett. **68**, 2076 (1996).
[18] V. Huard *et al.*, Microel. Reliab. **45**, 83 (2005).
[19] T. Grasser *et al.*, *Proc. International Reliability Physics Symposium (IRPS)* (2011), pp. 1–4.
[20] A. Haggag *et al.*, *Proc. International Reliability Physics Symposium (IRPS)* (2001), pp. 271–279.
[21] J. McPherson, *Proc. International Reliability Physics Symposium (IRPS)* (2007), pp. 209–216.
[22] C. Guerin *et al.*, Journ. Appl. Phys. **105**, 114513 (2009).
[23] E. Li *et al.*, *Proc. International Reliability Physics Symposium (IRPS)* (1999), pp. 253–258.
[24] K. Rupp *et al.*, *Proc. International Electron Devices Meeting (IEDM)* (2011), pp. 789–792.
[25] S. Tyaginov *et al.*, Microelectronics Reliability **50**, 1267 (2010).
[26] G. Pobegen *et al.*, IEEE Electron Dev. Lett. **34**, 939 (2013).